# CYCLIC SHEAR BEHAVIOR OF REINFORCED CONCRETE HAUNCHED BEAMS

A. Tena-Colunga[1], H.I. Archundia-Aranda[1,2], A. Grande-Vega[3] and O.M. González-Cuevas[1]

## ABSTRACT

This paper presents the final research results and interpretations about the testing of prototype reinforced concrete haunched beams subjected to cyclic loading. Beams were designed to present shear failure. Beams had no shear reinforcement. These haunched beams are identical in geometry and reinforcement to a set of haunched beams previously tested under static loading. These additional cyclic testing allowed to fully validate a proposed equation to estimate the shear strength of reinforced concrete haunched beams, taking into account parameters such as the haunch angle, the concrete compressive strength, the shear reinforcement and the negative contribution of the inclined longitudinal reinforcement. From the obtained results, it can be observed that haunched beams have a different cyclic shear behavior with respect to prismatic beams, having higher deformation and energy dissipation capacities, among other reasons, because non-prismatic beams favor an arching action in the haunched length as the main resisting mechanism.

## Introduction

Reinforced concrete haunched beams (RCHB) are often used in mid-rise framed buildings in high-risk earthquake areas, such as Mexico City. In fact, haunched beams are used in Mexico City since the first half of the 20th century, as architects and engineers consider that they provide the following advantages with respect to prismatic beams under lateral loading: (a) a more efficient use of concrete and steel reinforcement, (b) the weight of the building can be reduced for a given lateral stiffness, (c) eases the placement of different facilities or equipment (electrical, air conditioning, sewage, etc.) and, d) aesthetics reasons. The main disadvantages of these elements are that special formwork and qualified workers are needed to build them. However, as workmanship is relatively cheap in Mexico compared to US and Canadian standards, mid-rise haunched beam framed buildings are often built in Mexico City, as depicted in Fig. 1, where a structure built recently is shown.

Despite the fact that RCHB are commonly used in mid-rise buildings in Mexico, there are no specific recommendations for haunched beams in the most recent reinforced concrete norms for MFDC (NTCC-04, 2004) that would insure the ductile detailing of these elements. In addition, the ACI-318 code, often used in Mexico as a reference standard, does not have specific provisions either. Although the Russian and German codes cover the design of RCHB in some detail (Mac Leod and Houmsi 1994), these codes are not readily available to engineers in Mexico. Therefore, as reported earlier, the design of RCHB has

---

[1]Professor, Departamento de Materiales, Universidad Autónoma Metropolitana, Mexico City, MEXICO 02200
[2]Ph. D. Candidate, Posgrado en Ingeniería, UNAM, Mexico City, MEXICO 02200
[3]Graduate Student, Posgrado en Ingeniería Estructural, Universidad Autónoma Metropolitana, Mexico City, MEXICO

been mostly left to the experience and judgment of structural engineers in professional practice, and this fact has lead to unreliable design practices under lateral loading, as ductile behavior is not insured (Tena-Colunga 1994).



Figure 1. RC buildings with haunched beams recently constructed in Mexico City.

In fact, structural engineers do not have available enough sources of information to help them design adequately ductile RCHB in areas of high seismic risk. There are few books related to the design of reinforced concrete structures including brief sections regarding the design of RCHB (Park and Paulay 1997, Mac Gregor 1997 and Nielson 1999). Perhaps the major problem is the absence of sufficient experimental research devoted to understand the behavior of RCHB under shear and flexure, in contrast with the reasonable analytical efforts already done with respect to the stiffness modeling (i.e., Tena-Colunga 1996). Surprisingly, there are just few experimental studies on RCHB reported during the last 25 years (Debaiky and El-Niema 1982, Stefanou 1983, El-Niema 1988, MacLeod and Houmsi 1994, Archundia-Aranda *et al.* 2005 and 2006a).

In order to insure the ductile behavior of RCHB from a conceptual and capacity design viewpoint, it is necessary to understand: (a) first, how RCHB resist shear forces under static and cyclic loadings and, (b) second, after preventing potential shear failures, how to insure ductile flexural behavior under static and cyclic loadings. Therefore, it is clear that in order to achieve this goal, it is important first to assess the shear behavior of RCHB with experimental evidence.

Some experimental information is available on the shear strength of RCHB under static loading, mainly: (a) the tests of RCHB with shear reinforcement reported by Debaiky and El-Niema (1982), El-Niema (1988) and Stefanou (1983) and, (b) the tests without shear reinforcement reported by MacLeod and Houmsi (1994). However, this information was not enough still. Therefore, an experimental and analytical study was carried out to complement previous studies under static loading while using the geometries and practices observed in buildings recently constructed in Mexico City (Archundia-Aranda *et al.* 2005 and 2006a, Tena-Colunga *et al.* 2006). As a second phase of the ongoing research, haunched beams identical in geometry and reinforcement to the set of haunched beams previously tested under static loading are being subjected to cyclic loading (Archundia-Aranda *et al.* 2006b).

This paper summarizes final research results and interpretations about the testing of five prototype reinforced concrete haunched beams with no shear reinforcement subjected to cyclic loading, as described in following sections.

## Description of Test Beams

The geometry of prototype RCHB was defined according to a survey conducted in buildings of recent construction in Mexico City, as depicted in Fig. 2. The width for all beams was 22 cm. The effective span for all beams was $L$=2.80 m. The haunched length at both beam ends was one-third the effective span of the beam ($L_h=L/3 \approx 93.3$cm). The considered angles of slope of haunch from horizontal (or haunched

angle, α) were 0° (prismatic), 3.07°, 6.12°, 9.13° and 12.10°. The linear tapering was obtained by keeping a constant depth $h_{max}$=45 cm at the beam ends while varying the depth of the beam at the central third from 45 cm (prismatic) to 25 cm, that is, $h_{min}$=45, 40, 35, 30 and 25 cm).
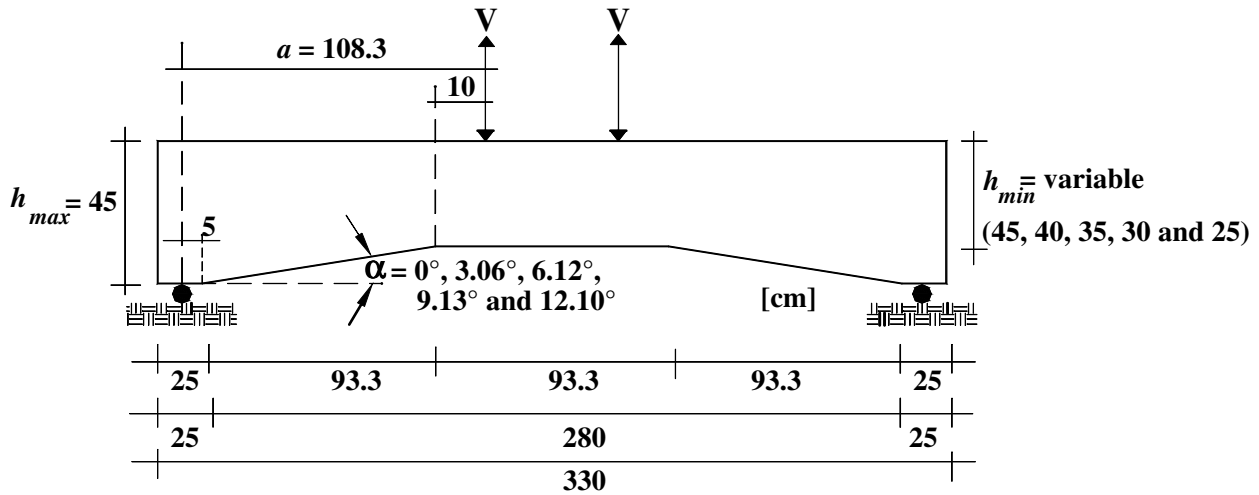


Figure 2. Geometry and loading for the test specimens.

The geometry of all beams satisfies the requirement $L/h_{max}$>5.0 to be considered as slender beam by NTCC-04. In addition, all beams satisfied the relation $a/d_{min}$> 2.5 (Wang and Salmon 1979) with the purpose of no magnifying the characteristic arching mechanism previously observed in RCHB (Debaiky and El-Niema 1982, MacLeod and Houmsi 1994).

The specified material properties for design were a nominal compressive strength $f'_c$=250 kg/cm$^2$ for the concrete and a yield tensile stress $f_y$=4200 kg/cm$^2$ for the steel reinforcement.

Two beams were constructed for each one of the five considered haunched angles α: a) a beam without shear reinforcement, only with four stirrups to hold the longitudinal steel reinforcement and, b) a beam with minimum shear reinforcement, equal to the one required by NTCC-04 for prismatic beams. Archundia-Aranda *et al.* (2005) present the details on how the specimens were designed while following general NTCC-04 guidelines but considering: a) the nominal contribution of concrete to shear ($V_c$) with an effective depth concept ($h_{eff}$), b) the nominal contribution of the steel reinforcement ($V_s$) and, c) the additional shear reinforcement in the vertex zone due to the abrupt change of direction of the bottom longitudinal reinforcement (Fig. 3).
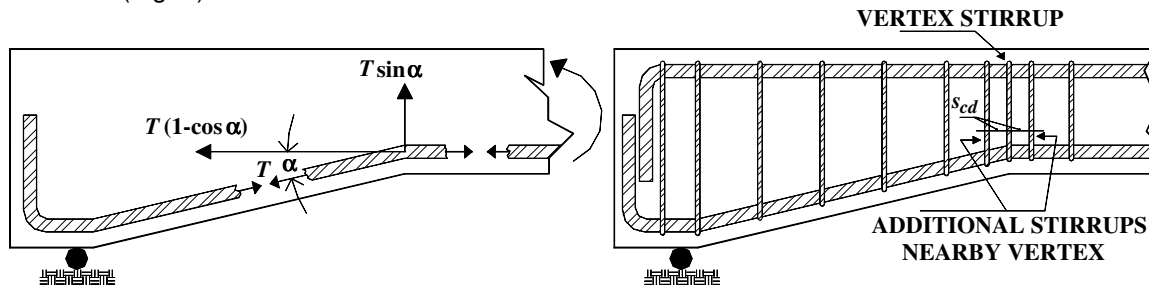


Figure 3. Additional shear reinforcement at the vertex zone due to the abrupt change of direction of the bottom longitudinal reinforcement.

The cryptogram for the identification of the beams for static loading is TASCα*i*-R*j*, where *i* is an index that indicates the considered haunched angle: *i*=0=0°, *i*=1=3.07°, *i*=2=6.12°, *i*=3=9.13° and *i*=4=12.10°; *j* is an

index that identifies the shear reinforcement: $j$=0 indicates the absence of shear reinforcement whereas $j$=1 indicates the use of minimum shear reinforcement as per NTCC-04. For cyclic loading, the cryptogram for identification is TASC$\alpha i$-R$j$-c, where the last $c$ indicates the cyclic loading. The reinforcement for each beam is summarized in Table 1. Typical reinforcement of beams with no shear reinforcement is depicted in Fig. 4.

Table 1. Identification of test specimens.

| Beam ID | $\alpha$ | Flexural reinforcement | | Shear reinforcement | | |
|---|---|---|---|---|---|---|
| | | Top | Bottom | Haunched length | Prismatic section | Vertex |
| TASC$\alpha$0-R0 TASC$\alpha$0-R0-c | 0° | 3#8 | 4#8 | 1 S#2.5 | 2 S#2.5 | - |
| TASC$\alpha$1-R0 TASC$\alpha$1-R0-c | 3.07° | 3#8 | 4#8 | 1 S#2.5 | 2 S#2.5 | - |
| TASC$\alpha$2-R0 TASC$\alpha$2-R0-c | 6.12° | 3#8 | 4#8 | 1 S#2.5 | 2 S#2.5 | - |
| TASC$\alpha$3-R0 TASC$\alpha$3-R0-c | 9.13° | 3#8 | 4#8 | 1 S#2.5 | 2 S#2.5 | - |
| TASC$\alpha$4-R0 TASC$\alpha$4-R0-c | 12.10° | 3#8 | 4#8 | 1 S#2.5 | 2 S#2.5 | - |
| TASC$\alpha$0-R1 TASC$\alpha$0-R1-c | 0° | 3#8 | 4#8 | 7S#2.5 @ 18.5 cm | 2S#2.5 @ 18.5 cm | 3S#2.5 @ 18.5 cm |
| TASC$\alpha$1-R1 TASC$\alpha$1-R1-c | 3.07° | 3#8 | 4#8 | 7S#2.5 @ 18.5 cm | 2S#2.5 @ 18.5 cm | 3S#2.5 @ 18.5 cm |
| TASC$\alpha$2-R1 TASC$\alpha$2-R1-c | 6.12° | 3#8 | 4#8 | 7S#2.5 @ 18.5 cm | 2S#2.5 @ 18.5 cm | 3S#2.5 @ 14 cm |
| TASC$\alpha$3-R1 TASC$\alpha$3-R1-c | 9.13° | 3#8 | 4#8 | 7S#2.5 @ 18.5 cm | 2S#2.5 @ 18.5 cm | 3S#2.5 @ 7.5 cm |
| TASC$\alpha$4-R1 TASC$\alpha$4-R1-c | 12.10° | 3#8 | 4#8 | 7S#2.5 @ 18.5 cm | 2S#2.5@ 18.5 cm | 3S#2.5 @ 4.5 cm |
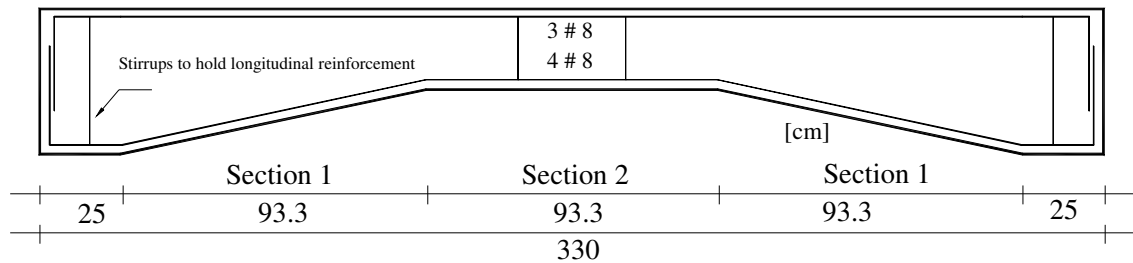


Figure 4. Reinforcement for beams TASC$\alpha$4-R0 and TASC$\alpha$4-R0-c.

**Instrumentation and Test Displacement History**

Beams were simply supported and tested under monotonic and cyclic loading ($V$) that were applied 10 cm from the vertex formed by the intersection of tapered sections with the prismatic section, as depicted in Fig. 2. The experimental setting for cyclic loading is depicted in Fig. 5b. External instrumentation for cyclic loading was designed to measure vertical deflections at midspan (two micrometers, one to measure deflections of the beams with respect to the reaction beam and one to measure the deflection of the reaction beam with respect to the ground floor, to correct beam deflections) and the applied loads with 4 load cells (Fig. 5b).

Cyclic tests were displacement-controlled in terms of the measured displacement at midspan $\delta$. According to previous results of monotonic tests, midspan displacement increments of 3 mm were set in the displacement history to allow capture first shear cracking and failure states. Two cycles at the same midspan displacement were set in the displacement history, as schematically depicted in Fig. 5b. This was done in order to evaluate key structural parameters such as stiffness and strength degradation, energy dissipation, equivalent viscous damping, damage indexes, etc. In Fig. 5b, positive displacements are obtained by applying the load downward.
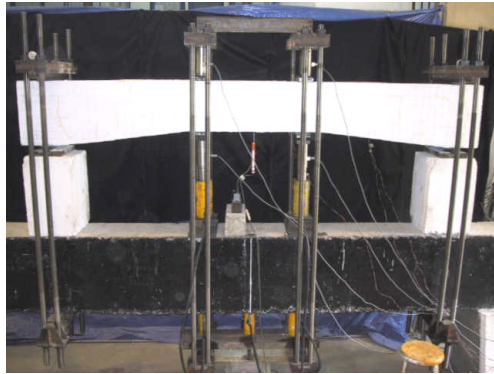


a) Testing setup
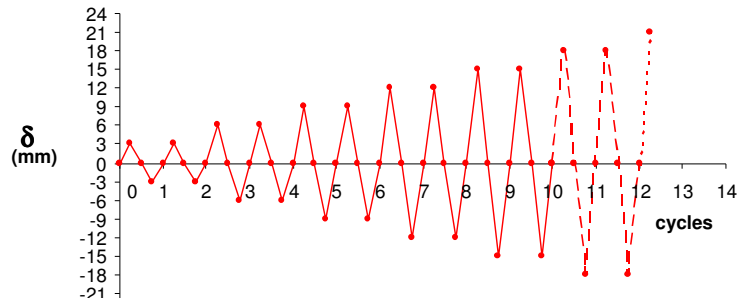


b) Cyclic displacement history

Figure 5.Testing setup and displacement history for cyclic loading.

In order to assess the contribution of the steel reinforcement, beams were internally instrumented with strain gages to measure tensional and compressional strains in the longitudinal steel reinforcement at half the haunched length, as schematically depicted in Fig. 6.
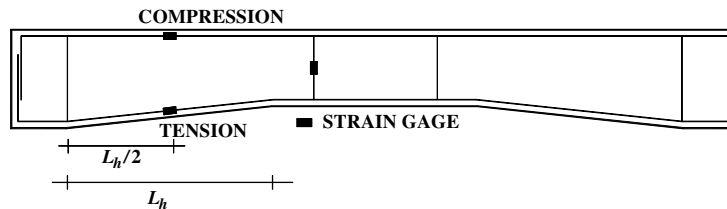


Figure 6. Typical internal instrumentation for beams TASC$\alpha$i-R0-c.

**Test Results**

The following results have been obtained, processed and compared from test results: (a) hysteretic curves (applied shear vs corrected midspan deflection $\delta$), (b) Characteristic shear forces and deflections for first diagonal cracking ($V_{cr}$ and $\delta_{cr}$), for collapse prevention ($V_u$ and $\delta_u$) and for collapse ($V_{collapse}$ and $\delta_{collapse}$), as described later, (c) V-$\delta$ envelopes for first and second cycles of response, (d) Deformation capacities, (e) Stiffness degradation for first and second cycles, (f) Energy dissipation characteristics for first and second cycles, (g) Equivalent viscous damping for first and second cycles, (h) Assessment of cracking patterns with damage states, (i) Assessment of Park-Ang damage index for RC haunched beams without shear reinforcement, (j) Assessment of the participation of the longitudinal reinforcement and, (k) Assessment of the formula formerly proposed to estimate the nominal shear strength of RCHB, based on previous static tests conducted by the authors and other researchers (i.e., Archundia-Aranda *et al.* 2005 and 2006a, Tena-Colunga *et al.* 2006). Because of space constrains, in this paper only few of these results will be presented and discussed, but they have been already reported and discussed in greater detail in Archundia-Aranda *et al.* (2006b).

**Hysteretic Curves and Damage States**

The hysteretic curves obtained for the five test specimens are depicted in Fig. 7, drawn at the same scale. It can be observed that for the geometry of the RCHB of this study, when the haunched angle increases, the volume of concrete diminishes, therefore, the shear strength also diminishes, as reported for monotonic tests (Archundia-Aranda *et al.* 2005 and 2006a, Tena-Colunga *et al.* 2006).

Although RCHB developed smaller ultimate shear strengths ($V_u$) with respect to the prismatic beam of reference (TASCα0-R0-c), haunched beams exhibited a greater deformation and energy dissipation capacity. This increment is primarily related to the capacity of RCHB to redistribute cracking along the haunched length (Fig. 8). The better cracking distribution (i.e., Fig. 8b) allowed that the ultimate shear strength $V_u$ did not suddenly happened after the appearance of the first important diagonal crack, as it happened for prismatic beams in both monotonic and cyclic tests (Fig. 8a). The observed behavior for RCHB is less brittle than for prismatic beams, as the shear failure for RCHB is noticeably less sudden than the one presented in prismatic beams.
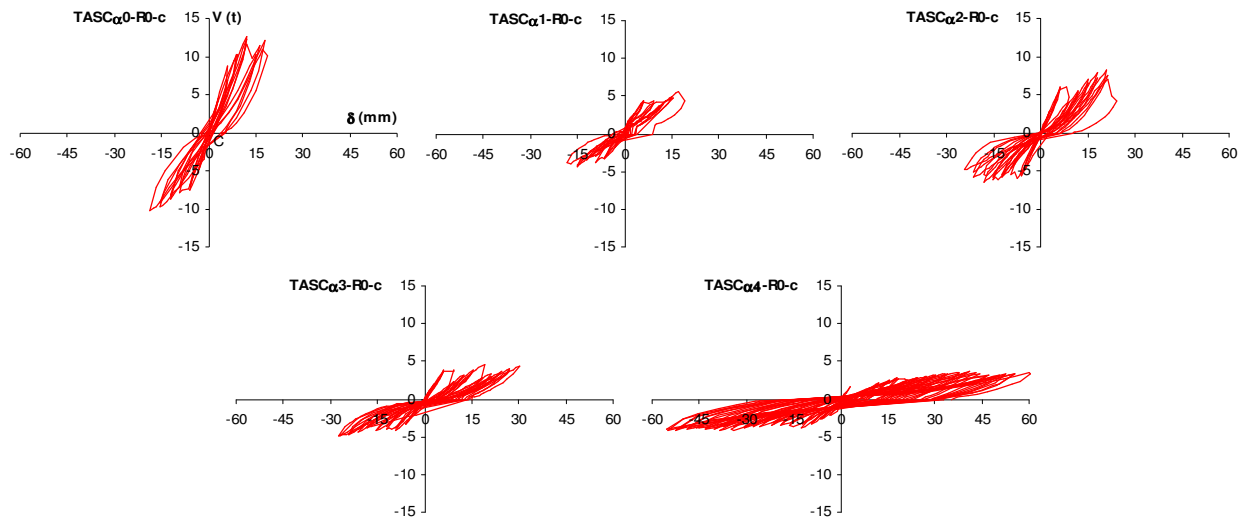


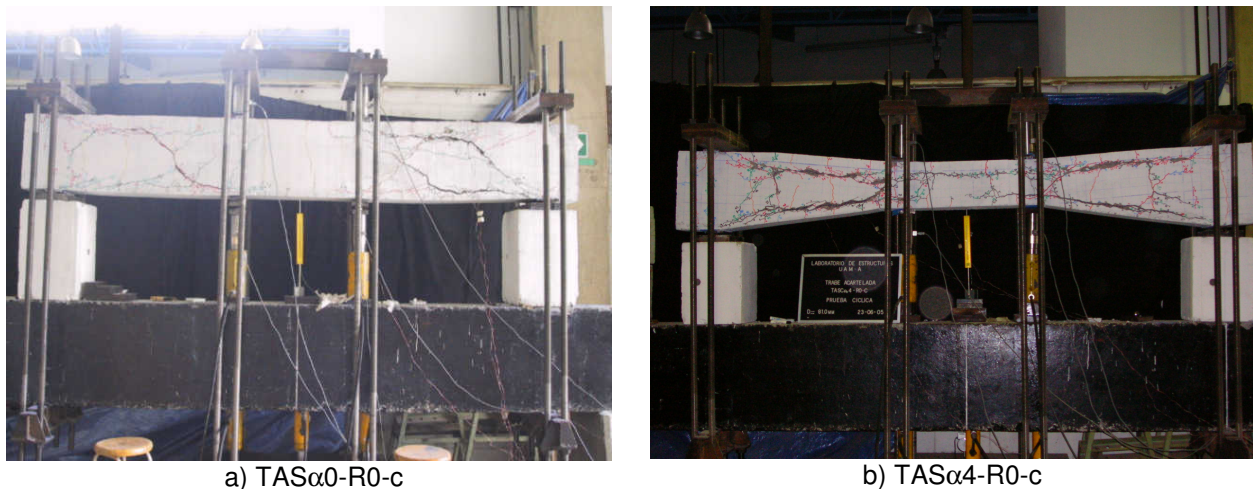Figure 7. Hysteretic curves for beams TASCαi-R0-c.



a) TASα0-R0-c

b) TASα4-R0-c

Figure 8. Final damage patterns for beams TASCαi-R0-c (at collapse state).

In addition, one can observe from the hysteretic curves depicted in Fig. 7 that as the haunch angle α increases, a pinching behavior is more pronounced due to the sliding along shear cracks. Due to the geometry of haunch beams, an slight asymmetric strength behavior is observed in the hysteretic loops (more noticeable for beam TASCα2-R0-c), as the inclined longitudinal reinforcement participates in a positive or negative way in resisting shear depending if the beam is pushed upward or downward.

Three damage states were defined during testing, as illustrated in Fig. 9: (1) First diagonal cracking (Fig. 9a), (2) Failure state, defined as the brittle state where a sudden diagonal crack is formed and the stiffness and strength of the element is considerably degraded afterwards, but repair is feasible (Fig. 9b) and, (3) Collapse state, the ultimate state that the beams developed (Figs. 9c and 8c).



| a) First Cracking | b) Failure | c) Collapse |

Figure 9. Defined damage states for beams TASCαi-R0-c (illustrated with TASCα3-R0-c).

During the testing it was confirmed the arch mechanism (Fig. 9b) reported in the monotonic tests (Archundia *et al.* 2005 and 2006a, Tena-Colunga *et al.* 2006) and by Debaiky and El-Niema (1982) for RCHB with shear reinforcement and MacLeod and Houmsi (1994) for RCHB without shear reinforcement. This arch mechanism was pronounced by the presence, in each haunch, of inclined compression struts. The struts tend to form between the point of application of the load and the midpoint of the haunched length.

**Peak Response Envelopes**

Load-displacement envelopes for peak responses obtained for the first and second cycles of deformation are depicted in Fig. 10 for the five test specimens. In this curves it can be confirmed that as the haunched angle increases: (a) deformation capacity increases and (b) shear strength is reduced. It is worth noting that beam TASCα1-R0-c ($3^0$) presented an anomalous brittle failure at a smaller shear force than TASCα2-R0-c ($6^0$), as in the monotonic tests it was always observed that the shear strength was reduced as the haunched angle α increased. First diagonal cracking occurred in most beams at a displacement around 6 mm (Table 2), except for beam TASCα4-R0-c ($12^0$), where first cracking occurred at 3 mm. Shear strength and displacements related to the three damage states previously defined (Fig. 9) obtained from the cyclic tests are reported in Table 2.
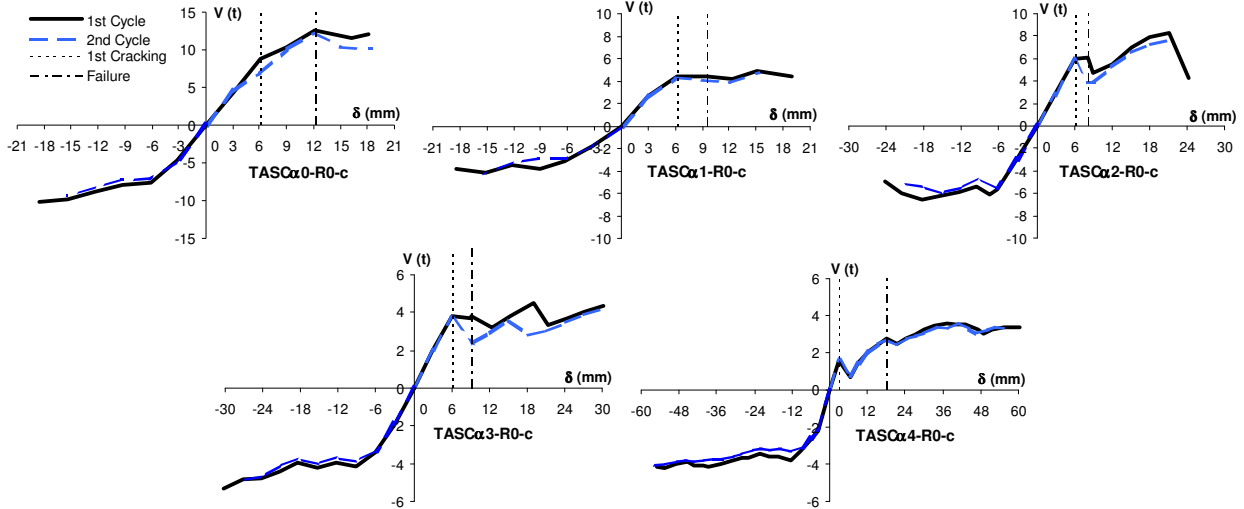
Figure 10. Load-displacement envelope curves for beams TASCαi-R0-c.

It can also be observed from the load-displacement envelopes depicted in Fig. 10 that the envelopes for first and second cycles start to differ after the major crack is formed at the failure state (Fig. 9b), although this difference is smaller for beams TASCα1-R0-c ($3^0$) and TASCα4-R0-c ($12^0$).

Table 2. Measured experimental shear forces and displacements related to failure states.

| ELEMENT | $\delta_{cr}$ (mm) | $\delta_u$ (mm) | $\delta_{collapse}$ (mm) | $V_{cr}$ (t) | $V_u$ (t) | $V_{collapse}$ (t) |
|---|---|---|---|---|---|---|
| TASCα0-R0-C | 6.06 | 12.10 | 18.10 | 8.78 | 12.61 | 12.06 |
| TASCα1-R0-c | 6.12 | 9.48 | 19.00 | 4.41 | 4.41 | 4.41 |
| TASCα2-R0-c | 6.14 | 8.88 | 24.30 | 5.97 | 6.08 | 4.21 |
| TASCα3-R0-c | 6.10 | 9.22 | 30.22 | 3.83 | 3.85 | 4.37 |
| TASCα4-R0-c | 3.08 | 18.14 | 60.46 | 1.61 | 2.76 | 3.41 |

**Stiffness Degradation**

Peak-to-peak secant stiffnesses were computed for each beam for each cycle of deformation as depicted in Fig. 11 and then these secant stiffnesses were normalized with respect to the initial elastic stiffness of each beams ($K/K_0$). In Figs. 12 and 13 it is depicted how the normalized secant stiffness $K/K_0$ decreases as the vertical displacement $\delta$ increases for all beam specimens. It can be observed from Fig. 13 that the effective secant stiffness for the first cycles of deformation is generally higher than for the second cycles of response for all beams.
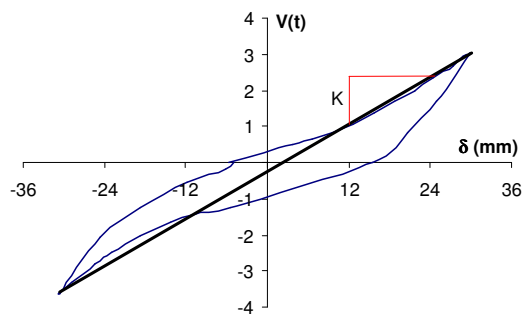


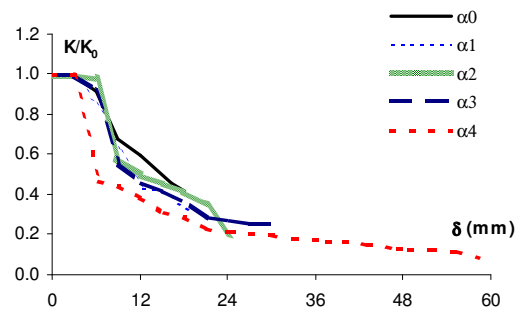Figure 11. Peak-to-peak secant stiffness K.
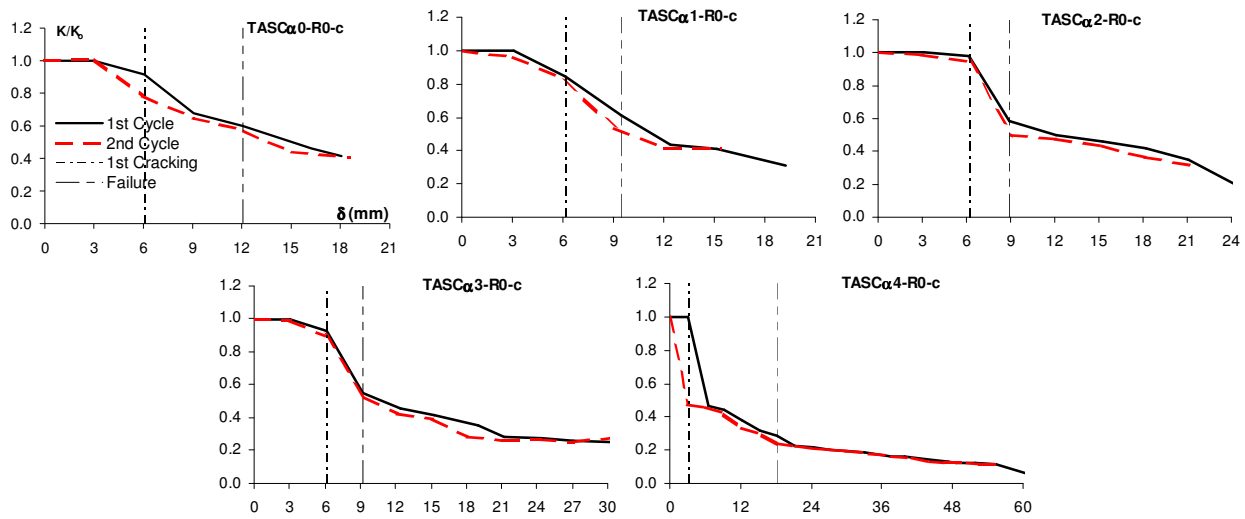


Figure 12. Stiffness degradation for beams TASCαi-R0-c.

1134

Figure 13. Normalized peak-to-peak secant stiffness curves for beams TASCαi-R0-c.

The value of the normalized secant stiffness for the three damage states previously defined (Fig. 9) are reported in Table 3. It can be observed that for most beams the stiffness degradation is small when the first cracks appears ($K_{cr}/K_0$). However, the effective stiffness is about 60% for most specimens when the sudden diagonal crack that defines the failure state appears (Fig. 9b), except for beam TASCα4-R0-c, where the effective stiffness is only 28% the initial elastic stiffness. These $K_u/K_0$ ratios are very similar to those obtained from the monotonic tests (Archundia-Aranda et al. 2005 and 2006a).

Table 3. Normalized peak-to peak secant stiffness.

| ELEMENT | $\alpha$ | $K_0$ (ton/mm) | $K_{cr}/K_0$ | $K_u/K_0$ | $K_{collapse}/K_0$ |
|---|---|---|---|---|---|
| TASCα0-R0-C | 0° | 1.46 | 0.92 | 0.60 | 0.42 |
| TASCα1-R0-c | 3.07° | 0.72 | 0.85 | 0.61 | 0.31 |
| TASCα2-R0-c | 6.12° | 0.95 | 0.98 | 0.58 | 0.20 |
| TASCα3-R0-c | 9.13° | 0.64 | 0.92 | 0.55 | 0.25 |
| TASCα4-R0-c | 12.10° | 0.57 | 0.98 | 0.28 | 0.18 |

## Equivalent Viscous Damping

Equivalent viscous damping were computed for each cycle of response from the hysteretic curves according to classic theory (i.e., Clough and Penzien 1993) and the resulting curves are shown in Fig. 13 for all beams, where a line is drawn for $\zeta=5\%$, commonly assumed for RC structures for analyses purposes. It can be observed that: a) before cracking, equivalent viscous damping is between 2% and 3%, b) after the first diagonal crack develops, effective damping is above 5%, c) peaks tend to form when an important crack develops or appear, d) the damping curves for the second cycles are mostly below the curves for the first cycles, as in the experiments the important cracks usually developed in the first deformation cycles and e) beam TASCα4-R0-c dissipates much more energy and therefore has a higher equivalent viscous damping after the first cracking compared with the other 4 beam specimens. It can be concluded from these curves that the 5% damping assumption is conservative enough when cracking is expected in RC elements, but it is high when elastic response is assumed.
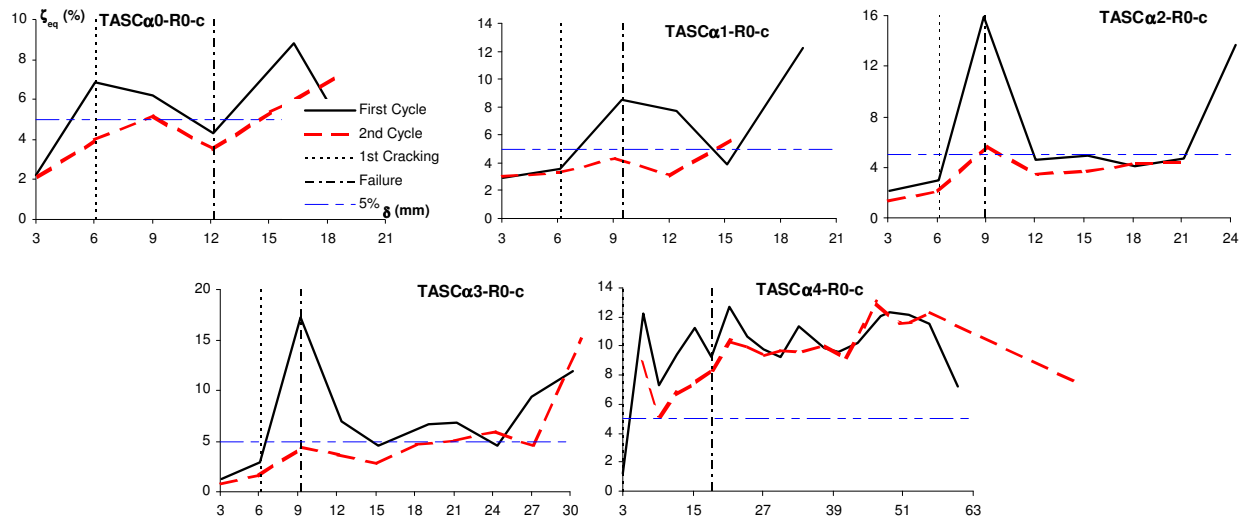
Figure 14. Equivalent viscous damping $\zeta_{eq}$ for beams TASC$\alpha$i-R0-c.

## Conclusions

From the analysis of experimental results of four haunched beams without transverse shear reinforcement tested under cyclic loading it is observed that the presence of a haunch modifies the brittle shear failure mode with respect to the prismatic element of reference. The presence of a haunch modifies important structural properties such as ultimate strength and deformation capacity, stiffness, energy dissipation and equivalent viscous damping. it was obtained that haunched beams have a different cyclic shear behavior with respect to prismatic beams, having higher deformation and energy dissipation capacities, among other reasons, because non-prismatic beams favor an arching action in the haunched length as the main resisting mechanism.

## References

Archundia-Aranda, H. I., A. Tena-Colunga and O. M. González-Cuevas, 2005. Estudio experimental del cortante estático en trabes acarteladas de concreto reforzado, *Reporte de Investigación 453*, División de Ciencias Básicas e Ingeniería, Universidad Autónoma Metropolitana, México, June, ISBN 970-31-0491-6 (in Spanish).

Archundia-Aranda, H. I, A. Tena-Colunga, A. and O. M. González-Cuevas, 2006a. Mecanismos de resistencia y deformación a cortante de trabes acarteladas de concreto reforzado, *Revista Internacional de Ingeniería en Estructuras* 11(1) 1-23 (in Spanish).

Archundia-Aranda, H. I., A. Tena-Colunga, A. Grande-Vega and O. M. González-Cuevas, 2006b. Cortante en trabes acarteladas de concreto reforzado sin refuerzo transversal sujetas a carga cíclica, *Proceedings, XV Congreso Nacional de Ingeniería Estructural*, Puerto Vallarta, Mexico, CDROM, 1-27, November (in Spanish).

Clough, R. W. and J. Penzien, 1993. *Dynamics of structures*, second edition, McGraw-Hill, USA.

Debaiky, S. Y. and E. I. El-Niema, 1982. Behavior and strength of reinforced concrete haunched beams in shear, *ACI Journal* 79 (3), 184-194.

El-Niema, E. I., 1988. Investigation of concrete haunched beams under shear, *ASCE Structural Journal* 114(4), 917-930.

MacGregor, J. G., 1997. *Reinforced concrete: Mechanics and design*, third edition, Prentice Hall, USA.

MacLeod, I. A. and A. Houmsi, 1994. Shear strength of haunched beams without shear reinforcement, *ACI Structural Journal* 91(1) 79-89.

Nilson, A. H., 1999. *Diseño de estructuras de concreto*, twelfth edition, Mc Graw Hill, Colombia, 132-133.

NTCC-2004, 2004. Normas Técnicas Complementarias para Diseño y Construcción de Estructuras de Concreto, *Gaceta Oficial del Distrito Federal*, México, October (in Spanish).

Park, R. and T. Paulay, 1997. *Estructuras de concreto reforzado*, Ninth printing of the first edition, Limusa, México, 279-284, 691-692 (in Spanish).

Stefanou, G. D., 1983. Shear resistance for reinforced concrete beams with non-prismatic sections, *Engineering Fracture Mechanics* 18(3), 643-667.

Tena-Colunga, A., 1994. Concerns regarding the seismic design of RC haunched beams, *ACI Structural Journal* 91(3) 287-293.

Tena-Colunga, A., 1996. Stiffness formulation for nonprismatic beam elements, *ASCE Journal of Structural Engineering* 122(12) 1484-1489.

Tena-Colunga, A., H. I. Archundia-Aranda and O. M. González-Cuevas, 2006. Shear strength and deformation of reinforced concrete haunched beams, in preparation to be submitted to *ACI Structural Journal or Engineering Structures*.

Wang, C. K and C. G. Salmon, 1979. *Reinforced concrete design*, third edition, Harper and Row Publishers, USA.